

Electrostatic Force and Torque Description of Generalized Spheroidal Particles in Optical Landscapes

Ryan W. Going, Brandon L. Conover, Michael J. Escuti

North Carolina State Univ, Dept Electrical & Computer Engineering, Raleigh (USA)

ABSTRACT

Optical trapping, mixing, and sorting of micro- and nano-scale particles of arbitrary shape (e.g., blood cells and nanorods) are but a few of the burgeoning applications of optical interference landscapes. Due to their non-invasive, non-contact manipulation potential, biologists and nanotechnologists alike are showing increased interest in this area and experimental results continue to be promising. A complete and reliable theoretical description of the particles' response within these fields will allow us to accurately predict their behavior and motion. We develop an electrostatic model of the optical force and torque on anisotropic particles in optical intensity gradients. The complete optical field is defined and a Maxwell stress tensor approach is taken to realize the force and torque induced by the electric field due to the polarizability of the particle. We utilize the properties of real dielectrics and steady state optical fields to extend this approach to the electrodynamic case inherent in optical trapping. We then compare our results against our recently reported form factor approach and use the differences to try to determine the importance of polarizability in optical trapping.

Keywords: Optical Trapping, Spheroidal Harmonics, Maxwell Stress Tensor

1. INTRODUCTION

Since the gradient force optical trap was demonstrated by Ashkin and associates in 1986,¹ the ability to manipulate dielectric particles with light has made great advancement. Experimental work has promised to make optical traps an industry tool, not simply a magical laboratory demonstration.² Biological particle sorting,³ nano-assembly,⁴ and studies of fundamental interactions between cells and molecules show just how far this important technique can travel. In order to fully harness this new technology, however, a fundamental theoretical understanding is first required.

While there has been a significant theoretical treatment of trapping simple shapes such as spheres and cylinders⁵⁻⁷ there has been very little study of particles with other common shapes (spheroids, ellipsoids, wires, etc.) beyond a few studies of optically-induced torque and constrained motion.^{8,9} The study of non-spherical dielectrics is quite important because the majority of particles in practical settings (e.g., blood cells, nanowires) are modeled better as shapes more complex than spheres. For those particles much smaller than the illuminating wavelength (Rayleigh particles), a dipole model may be used to calculate the resultant forces, while for particles much larger (Mie particles), a ray optics model is often used. However, when the particle size is on the order of the illuminating wavelength, neither of these approximations hold true and more complete electromagnetic treatment is required. To this end, continuous form factor models have been developed to provide analytic expressions for the optically-induced force¹⁰ and torque¹¹ on dielectrics of varying size and shape. While results show promise, a more rigorous treatment encompassing all arbitrary particles and fields is still needed.

We calculate the response of a spheroidal dielectric in an arbitrary optical field using the well-known Maxwell stress tensor (MST) method.¹²⁻¹⁴ In order to calculate the electric field, we make use of spheroidal harmonics to solve the Laplace equation. We first take an electrostatic approach in solving the MST and then take advantage of the properties of real dielectrics and steady-state optical fields to apply this to the electrodynamic case of optical trapping. This approach lends itself to a complete study of the effects of field polarization as it pertains to optical manipulation. Finally, we compare results of our MST model to those of the form factor models.

Correspondence should be addressed to: mjescuti@ncsu.edu, +1 919 513 7363

2. BACKGROUND

2.1 Maxwell Stress Tensor

Due to the size regime of interest for optical trapping, where the wavelength of light used is on the order of the size of the particle, the ray and dipole approximations both fail. Instead the MST, which is well known to be accurate for all sizes and shapes of particles, should be used. Force (\mathbf{F}) and torque (\mathbf{M}) can be calculated using the MST, \mathbf{T} as below.^{15, 16} Note that in the approach here, we will employ an electrostatic model (i.e. no time variation of electromagnetic fields) that we will generalize in a final step to apply to steady-state electrodynamic fields of interest (time varying waves at optical frequencies). In addition we assume a real dielectric particle which is non-magnetic, and thus the magnetic field is not included in the MST as its force and torque contributions are zero.

$$\mathbf{T} = \begin{bmatrix} T_{xx} & T_{xy} & T_{xz} \\ T_{yx} & T_{yy} & T_{yz} \\ T_{zx} & T_{zy} & T_{zz} \end{bmatrix} \quad (1)$$

$$T_{\alpha\beta} = \frac{1}{2} \mathbf{Re} \left\{ \epsilon_m E_\alpha^* E_\beta - \frac{1}{2} \epsilon_m |\mathbf{E}|^2 \delta_{\alpha\beta} \right\}, \quad \alpha, \beta \in x, y, z \quad (2)$$

$$\mathbf{F} = \int_s \mathbf{T} \cdot \hat{\mathbf{n}} \, dA \quad (3)$$

$$\mathbf{M} = \int_s \mathbf{r} \times (\mathbf{T} \cdot \hat{\mathbf{n}}) \, dA \quad (4)$$

where ϵ_m is the permittivity of the medium surrounding the particle, \mathbf{r} is the radial vector from the center of the particle to the points on the surface, $\hat{\mathbf{n}}$ is the unit normal vector on the surface of the spheroid, and dA is the surface element. Note that $\delta_{\alpha\beta}$ refers to the Dirac Delta function, where $\delta_{\alpha\beta} = 1$ if $\alpha = \beta$ and $\delta_{\alpha\beta} = 0$ if $\alpha \neq \beta$. When the electric field is multiplied by its complex conjugate as in (2) and the real component taken, the time dependent portion of the field essentially cancels out. Thus the Maxwell stress tensor in this form gives a time-averaged value.

Solving for the electric field, a potential internal to the particle is induced due to an applied potential when there is a difference in permittivities between the particle and the surrounding medium. From first principles, the internal and external potentials must obey the Laplace equation.^{17, 18} At the spheroidal surface boundary, the potentials must also obey a basic set of boundary conditions. Namely, the potential must be continuous across the boundary and the displacement in the normal direction to the boundary surface must be continuous:¹⁹

$$\Phi_i = \Phi_e|_{\text{boundary}} \quad (5)$$

$$\epsilon_r \frac{d}{d\mathbf{n}} \Phi_i = \frac{d}{d\mathbf{n}} \Phi_e \Big|_{\text{boundary}} \quad (6)$$

where Φ_i and Φ_e represent the internal and external potential functions respectively, ϵ_p is the permittivity of the particle, and $\epsilon_r = \epsilon_p/\epsilon_m$ is the ratio of particle and medium permittivities. In order to easily solve the boundary conditions, we make use of the spheroidal coordinate system,^{20, 21} defined in terms of the cartesian coordinates local to the particle's frame of reference x', y', z' :

$$x' = h \cosh \eta \sin \theta \cos \phi \quad (7a)$$

$$y' = h \cosh \eta \sin \theta \sin \phi \quad (7b)$$

$$z' = h \sinh \eta \cos \theta \quad (7c)$$

and seen related in Fig. 1. The constant h is calculated in terms of the fundamental spheroid for the system. We take advantage of the spheroidal symmetry of the particle where a is the semidiameter along the axis of rotation and b is the semidiameter along both orthogonal axes. Thus, h is found by

$$h = \sqrt{a^2 - b^2} \quad (8)$$

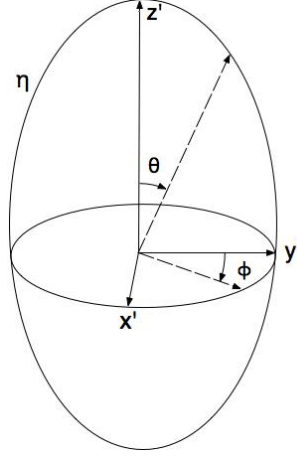


Figure 1. Spheroidal Coordinate system in relation to the cartesian axes. ϕ is the azimuthal angle, and spans the $x'y'$ plane with a range of $[0, 2\pi]$. θ is the polar angle with a range of $[0, \pi]$. η is the radial variable with range $[0, \infty)$.

Another important quantity is that of the fundamental spheroid, defined by constant η_0 . When $\eta = \eta_0$, the other two coordinates, θ and ϕ span the surface of the fundamental spheroid and hence the surface of the particle of interest. It is important to define the value of η_0 :

$$\eta_0 = \cosh^{-1} \left(\frac{a}{\sqrt{a^2 - b^2}} \right) \quad (9)$$

2.2 Spheroidal Harmonic Functions

The potential function is subject to satisfying the Laplace equation, and hence is a harmonic function. Since our system contains spheroidal boundaries, we are most interested in the spheroidal harmonic functions. The spheroidal harmonics are an orthonormal basis which can represent any potential function defined on a spheroidal surface.²¹ They are made up of harmonics of the first and second kind defined respectively as follows:

$$\sum_{n=1}^{\infty} \sum_{p=0}^n Y_n^p(\theta, \phi) \frac{P_n^p(\cosh \eta)}{P_n^p(\cosh \eta_0)} \quad (10)$$

$$\sum_{n=1}^{\infty} \sum_{p=0}^n Y_n^p(\theta, \phi) \frac{Q_n^p(\cosh \eta)}{Q_n^p(\cosh \eta_0)} \quad (11)$$

$$Y_n^p(\theta, \phi) = \frac{2(2n+1)(n-p)!}{4\pi(n+p)!} P_n^p(\cos \theta) (C_{np} \cos p\phi + S_{np} \sin p\phi) \quad (12)$$

Where P_n^p and Q_n^p are the associated Legendre functions of the first and second kind respectively. Note that Eq. (12) is reduced by a factor of 2 when $p = 0$. The C_{np} and S_{np} are specific to a given function, $f(\eta, \theta, \phi)$ and are determined by a finite integral formula. Here $f(\eta, \theta, \phi)$ represents any general function parameterized with spheroidal coordinates, and the applied potential will be substituted for this later on.

$$C_{np} = \int_0^\pi \int_0^{2\pi} f(\eta_0, \theta, \phi) P_n^p(\cos \theta) \cos p\phi \sin \theta d\phi d\theta \quad (13)$$

$$S_{np} = \int_0^\pi \int_0^{2\pi} f(\eta_0, \theta, \phi) P_n^p(\cos \theta) \sin p\phi \sin \theta d\phi d\theta \quad (14)$$

We can use this series expansion to represent the applied electric potential function, Φ_0 , which has been parameterized in terms of spheroidal coordinates. Putting all this together creates a spheroidal harmonic representation of the function Φ_0 . It should be noted that the s and c found in the constants K_{np}^s, K_{np}^c are labels and do not correspond to any variables or constants.

$$\Phi_0 = \sum_{n=1}^{\infty} \sum_{p=0}^n \frac{2(2n+1)(n-p)!}{4\pi(n+p)!} P_n^p(\cos\theta) (K_{np}^c \cos p\phi + K_{np}^s \sin p\phi) \frac{P_n^p(\cosh\eta)}{P_n^p(\cosh\eta_0)} \quad (15)$$

$$K_{np}^c = \int_0^\pi \int_0^{2\pi} \Phi_0(\eta_0, \theta, \phi) P_n^p(\cos\theta) \cos p\phi \sin\theta d\phi d\theta \quad (16)$$

$$K_{np}^s = \int_0^\pi \int_0^{2\pi} \Phi_0(\eta_0, \theta, \phi) P_n^p(\cos\theta) \sin p\phi \sin\theta d\phi d\theta \quad (17)$$

Note that when actually calculating values it is both impractical and impossible to carry out an infinite sum of terms, and as a crude rule of thumb a series carried out to $n = N$ is analogous to approximating a function with an N th order polynomial.

2.3 Solution of Laplace Equation

By employing spheroidal boundary conditions, our potential functions take the form of the spheroidal harmonics. Since the internal potential is defined everywhere inside the particle, the solution for the internal potential should include only the harmonics of the first kind. Furthermore, since it should decay as a function of distance from the particle, the externally induced potential should only contain harmonics of the second kind in addition to the applied potential. Thus the total internal and external potential functions are:

$$\Phi_i = \sum_{n=1}^{\infty} \sum_{p=0}^n \frac{2(2n+1)(n-p)!}{4\pi(n+p)!} P_n^p(\cos\theta) (A_{np}^c \cos p\phi + A_{np}^s \sin p\phi) \frac{P_n^p(\cosh\eta)}{P_n^p(\cosh\eta_0)}, \quad (18)$$

$$\begin{aligned} \Phi_e = & \sum_{n=1}^{\infty} \sum_{p=0}^n \frac{2(2n+1)(n-p)!}{4\pi(n+p)!} P_n^p(\cos\theta) (K_{np}^c \cos p\phi + K_{np}^s \sin p\phi) \frac{P_n^p(\cosh\eta)}{P_n^p(\cosh\eta_0)} \\ & + \sum_{n=1}^{\infty} \sum_{p=0}^n \frac{2(2n+1)(n-p)!}{4\pi(n+p)!} P_n^p(\cos\theta) (B_{np}^c \cos p\phi + B_{np}^s \sin p\phi) \frac{Q_n^p(\cosh\eta)}{Q_n^p(\cosh\eta_0)}, \end{aligned} \quad (19)$$

where the values of K_{np}^c and K_{np}^s are the same as Eqns. (16) and (17). The values of the coefficients $A_{np}^c, A_{np}^s, B_{np}^c$, and B_{np}^s must be determined from the boundary conditions. By substituting the above expressions in the boundary condition equations, and by utilizing the properties of orthogonal functions, the following set of equations result:

$$A_{np}^s = B_{np}^s + K_{np}^s \quad (20a)$$

$$A_{np}^c = B_{np}^c + K_{np}^c \quad (20b)$$

$$\epsilon_r A_{np}^s \frac{\partial}{\partial \eta} \frac{P_n^p(\cosh\eta)}{P_n^p(\cosh\eta_0)} = B_{np}^s \frac{\partial}{\partial \eta} \frac{Q_n^p(\cosh\eta)}{Q_n^p(\cosh\eta_0)} + K_{np}^s \frac{\partial}{\partial \eta} \frac{P_n^p(\cosh\eta)}{P_n^p(\cosh\eta_0)} \Big|_{\eta=\eta_0} \quad (20c)$$

$$\epsilon_r A_{np}^c \frac{\partial}{\partial \eta} \frac{P_n^p(\cosh\eta)}{P_n^p(\cosh\eta_0)} = B_{np}^c \frac{\partial}{\partial \eta} \frac{Q_n^p(\cosh\eta)}{Q_n^p(\cosh\eta_0)} + K_{np}^c \frac{\partial}{\partial \eta} \frac{P_n^p(\cosh\eta)}{P_n^p(\cosh\eta_0)} \Big|_{\eta=\eta_0} \quad (20d)$$

Solving these equations simultaneously gives a solution for the A_{np} and B_{np} coefficients in terms of the already known K_{np} coefficients. Note that the number of K_{np} terms found in the expansion explained Section 2.2 also

limits the number of terms used to describe the induced potentials. However, in nearly all cases, if there are enough expansion terms to adequately describe the applied potential, then that same number of terms will also adequately describe the induced potential. The final result for the relations of these coefficients is:

$$A_{np}^s = \frac{K_{np}^s(1+n-p)(P_{1+n}^p(\cosh \eta_0)Q_n^p(\cosh \eta_0) - P_n^p(\cosh \eta_0)Q_{1+n}^p(\cosh \eta_0))}{A_d} \quad (21a)$$

$$A_{np}^c = \frac{K_{np}^c(1+n-p)(P_{1+n}^p(\cosh \eta_0)Q_n^p(\cosh \eta_0) - P_n^p(\cosh \eta_0)Q_{1+n}^p(\cosh \eta_0))}{A_d} \quad (21b)$$

$$B_{np}^s = \frac{A_{np}^s(\epsilon_r - 1)((1+n)\cosh \eta_0 P_n^p(\cosh \eta_0) + (p-n-1)P_{1+n}^p(\cosh \eta_0))Q_n^p(\cosh \eta_0)}{(1+n-p)(P_{1+n}^p(\cosh \eta_0)Q_n^p(\cosh \eta_0) - P_n^p(\cosh \eta_0)Q_{1+n}^p(\cosh \eta_0))} \quad (21c)$$

$$B_{np}^c = \frac{A_{np}^c(\epsilon_r - 1)((1+n)\cosh \eta_0 P_n^p(\cosh \eta_0) + (p-n-1)P_{1+n}^p(\cosh \eta_0))Q_n^p(\cosh \eta_0)}{(1+n-p)(P_{1+n}^p(\cosh \eta_0)Q_n^p(\cosh \eta_0) - P_n^p(\cosh \eta_0)Q_{1+n}^p(\cosh \eta_0))} \quad (21d)$$

$$A_d = (1+n-p)\epsilon_r P_{1+n}^p(\cosh \eta_0)Q_n^p(\cosh \eta_0) - P_n^p(\cosh \eta_0)((1+n)(\epsilon_r - 1)\cosh \eta_0 Q_n^p(\cosh \eta_0) + (1+n-p)Q_{1+n}^p(\cosh \eta_0)) \quad (21e)$$

2.4 Conversion to Cartesian Electric Field

Since we need the actual electric field to evaluate the MST, we recall that

$$\mathbf{E} = -\nabla\Phi \quad (22)$$

Since the boundary conditions explicitly state $\Phi_i = \Phi_e$ at this surface, we can use either expression to find the electric field and Φ_i is chosen for simplicity. Also, since the spheroidal harmonic expression we have for the potential is in spheroidal coordinates, it is sensible to take the spheroidal gradient and then convert the spheroidal electric field vector to a cartesian vector. In the end we would like the force and torque vectors in cartesian unit vectors, and so this conversion is done at this point to accomplish this. The gradient in spheroidal coordinates is defined as follows:²⁰

$$\mathbf{E} = -\frac{1}{h\sqrt{\sinh^2 \eta + \sin^2 \theta}} \frac{\partial \Phi_i}{\partial \eta} \hat{\boldsymbol{\eta}} - \frac{1}{h\sqrt{\sinh^2 \eta + \sin^2 \theta}} \frac{\partial \Phi_i}{\partial \theta} \hat{\boldsymbol{\theta}} - \frac{1}{h \sinh \eta \sin \theta} \frac{\partial \Phi_i}{\partial \phi} \hat{\boldsymbol{\phi}} \quad (23)$$

To convert the electric field from a spheroidal vector to a cartesian vector, the following unit vector transformation matrix is used:

$$\begin{bmatrix} \hat{\mathbf{i}}' \\ \hat{\mathbf{j}}' \\ \hat{\mathbf{k}}' \end{bmatrix} = \begin{bmatrix} \frac{\cosh \eta \sin \theta \cos \phi}{\sqrt{\sinh^2 \eta + \sin^2 \theta}} & \frac{\cosh \eta \sin \theta \sin \phi}{\sqrt{\sinh^2 \eta + \sin^2 \theta}} & \frac{\sinh \eta \cos \theta}{\sqrt{\sinh^2 \eta + \sin^2 \theta}} \\ \frac{\sinh \eta \cos \theta \cos \phi}{\sqrt{\sinh^2 \eta + \sin^2 \theta}} & \frac{\sinh \eta \cos \theta \sin \phi}{\sqrt{\sinh^2 \eta + \sin^2 \theta}} & \frac{-\cosh \eta \sin \theta}{\sqrt{\sinh^2 \eta + \sin^2 \theta}} \\ -\sin \phi & \cos \phi & 0 \end{bmatrix}^{-1} \cdot \begin{bmatrix} \hat{\boldsymbol{\eta}} \\ \hat{\boldsymbol{\theta}} \\ \hat{\boldsymbol{\phi}} \end{bmatrix} \quad (24)$$

Since $\hat{\boldsymbol{\eta}}$ is the normal vector, it is simply transformed to a cartesian unit vector. The radial vector is also defined below. Also defined below is the surface element, dA . All of the vectors are parameterized by spheroidal coordinates for the purposes of integration.

$$\hat{\mathbf{n}} = \hat{\boldsymbol{\eta}} \quad (25a)$$

$$\mathbf{r} = h \cosh \eta \sin \theta \cos \phi \hat{\mathbf{i}}' + h \cosh \eta \sin \theta \sin \phi \hat{\mathbf{j}}' + h \sinh \eta \cos \theta \hat{\mathbf{k}}' \quad (25b)$$

$$dA = h^2 \sqrt{\sinh^2 \eta_0 + \sin^2 \theta} \sinh \eta_0 \sin \theta d\theta d\phi \quad (25c)$$

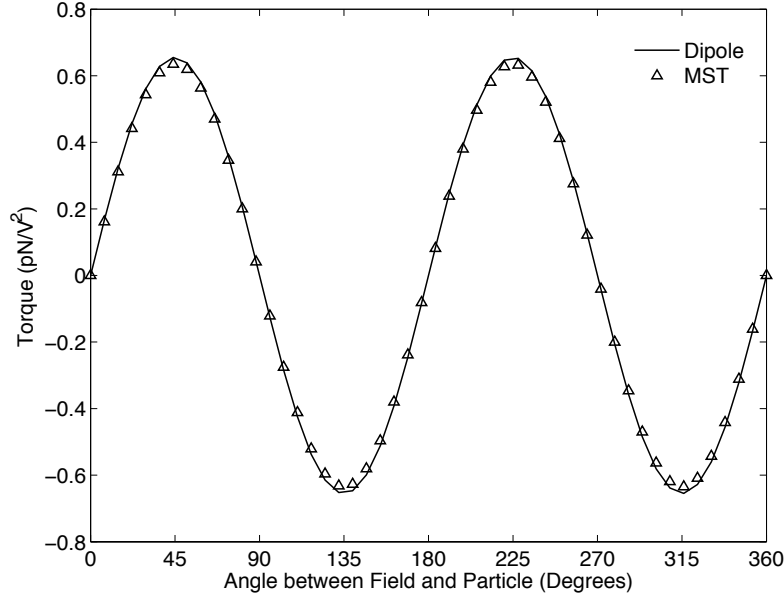


Figure 2. Comparison of Torque between Dipole Model and MST calculation for a constant electric field, normalized to values of E_0, a, b, ϵ_m .

2.5 Dipole Comparison

In order to at least partially validate the full MST method derived in Section 2.3, we compare its results to a more simple, but approximate, model based on a simple dipole within a spatially varying electric field. We examine the dipole model as described by Paul and Kaler.⁸ Their expressions for determining simple dipole torque given a spatially-varying potential can be found in their paper, and are not repeated here for the sake of brevity. First the potential is defined for an applied constant electric field:

$$\Phi_0 = E_0 (z' \cos \Omega - y' \sin \Omega) \quad (26a)$$

$$\mathbf{E}_0 = -\nabla \Phi_0 = E_0 \sin \Omega \hat{\mathbf{j}}' - E_0 \cos \Omega \hat{\mathbf{k}}' \quad (26b)$$

where Ω refers to the angle from the direction of electric field vector to the direction of the spheroid's symmetry axis vector. E_0 refers to the magnitude of the electric field. Using the methodology described in the previous sections, we calculate the specific K_{np}^s and K_{np}^c coefficients, find the A_{np}, B_{np} coefficients for the induced potentials, write the electric field, and calculate the force and torque. We expect two major results when using a constant electric field: all components of force will be zero and the values for torque should generally agree with those predicted by the dipole model. The first prediction of zero force is easily verified, and not shown in favor of more interesting data.

A comparison between the two methods can be seen in Figure 2, where torque is shown against the rotation of the particle within the constant electric field. The values of torque in each method have been normalized for E_0, a, b , and ϵ_m . It is apparent the two methods closely agree with each other. Any deviation between the two can be attributed to the dipole model being fully analytic, while our MST calculation contains inherent numerical error. However it is easily seen from the comparison that the amount of numerical error is quite small.

3. SINUSOIDAL LANDSCAPE

While this work deals primarily with an electrostatic system, the results can be applied to an electrodynamic case, such as that of a steady state optical system. Our chosen optical field is a 1D periodic optical landscape, created by simple holography. At optical frequencies, particles only respond to the time averaged force and torque, calculable via the stress tensor using the electric field phasor and its conjugate. This is valid because

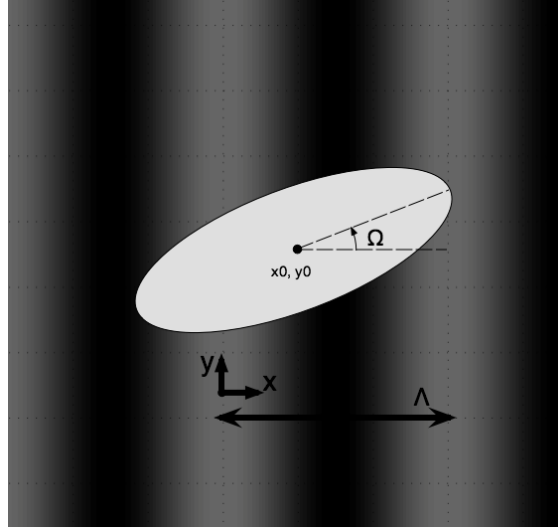


Figure 3. Definition of Parameters used in electric field and potential equations

we assume a real permittivity, that is, there is no time lag in the polarization of the particle.²² Combining this along the the MST form seen in Eq. (2) and the phasor notation for the electric field, it can be seen that the time component of the field drops out of the MST calculation. Thus writing the electric field in proper phasor notation combined with the proper MST formulation gives the proper time averaged result. We retain interest in non-magnetic particles only, allowing the magnetic field components to be neglected.

3.1 Potential Definition

It is important to know how we define the electric field and electric potential and how the particle is placed in this environment to understand the effects of the field on the particle. Referencing the setup shown in Figure 3, we first want the intensity, $I(x)$ to take the following form. We then arbitrarily pick the optical field to have a p-polarization, and placing this into the particle's local coordinate frame, we then get the following form for the electric field:

$$I(x) = I_0 \left(1 + \cos \frac{2\pi x}{\Lambda} \right) \quad (27)$$

$$\mathbf{E} = -E_0 \exp \left(i \frac{\pi}{\Lambda} x \right) \hat{\mathbf{i}} \quad (28)$$

where E_0 is the electric field magnitude, Λ is the intensity period of the field, Ω is the angle of particle rotation, x is the x -coordinate of the center of the particle in the global coordinate system. We can convert to the local coordinate system of the particle by using the transformation matrix described in Eq. (31).

Knowing that the electric field is simply the negative gradient of the potential, the potential takes the following form:

$$\Phi_0 = \frac{E_0 \Lambda}{i\pi} \exp \left(i \frac{\pi}{\Lambda} x \right) \quad (29)$$

The important features to note are that Ω marks the angle from the grating vector to symmetry axis of the spheroid. A positive Ω corresponds to a clockwise rotation of the field, which is equivalent to a counterclockwise rotation of the particle itself. The x_0/Λ term represents the normalized offset of the center of the particle from

the global origin in the x -direction. In addition, we use the following relation to correlate optical intensity, I_0 , with electric field magnitude, E_0 :

$$E_0 = \sqrt{2I_0 \sqrt{\frac{\mu_0}{\epsilon_m \epsilon_0}}} \quad (30)$$

Finally, in order to make useful the results of force and torque as calculated in the local coordinates of the particle, we introduce the following transformation to convert the force and torque into the global coordinates of the system as defined above.

$$\begin{bmatrix} \hat{\mathbf{i}} \\ \hat{\mathbf{j}} \\ \hat{\mathbf{k}} \end{bmatrix} = \begin{bmatrix} 0 & \sin \Omega & \cos \Omega \\ 0 & \cos \Omega & -\sin \Omega \\ -1 & 0 & 0 \end{bmatrix} \cdot \begin{bmatrix} \hat{\mathbf{i}}' \\ \hat{\mathbf{j}}' \\ \hat{\mathbf{k}}' \end{bmatrix} \quad (31)$$

3.2 Results of the MST Calculation

In order to analyze the results of the model in the case of a 1-D sinusoidal optical field, it is often most helpful to examine the results of sweeping across the major parameters in the system. We examine the results for force and torque against changes in x_0/Λ , Ω , and Λ . The relative particle position is first examined, as can be seen in Fig. 4. In the graph showing force, it can be seen that when the particle is centered on a bright fringe, $x_0/\Lambda = 0, 1$, or a dark fringe, $x_0/\Lambda = 0.5$, the x-component of force is 0. This means that a particle centered on a fringe is trapped within that 'pillar'. It should also be noticed that a particle centered on a dark fringe is in an unstable equilibrium, and that if its center is slightly off of a fringe, the particle experiences a force towards the nearest bright fringe. This generally agrees with assertions made in previous work. We would normally expect the y-component of force to be 0 since there is no field gradient in the y-direction, however the figure shows a definite force in the y-direction. This is likely due to the finite number of expansion terms of our spheroidal wavefunctions (in this simulation set to 6). Looking at the graph of torque, it can be seen that torque is maximized at the bright fringes, which should be expected as the field is at its maximum at these points. Also, the torque is minimized but non-zero at the dark fringe. What is most interesting to note is that the torque is always non-zero in our MST calculation, which is most likely due to the polarization of the field. What is seen is most likely a competition between torque on the particle from the intensity gradient, where the long axis of the particle tries to align with the fringes, and the polarization in the x-direction, where the long axis of the particle tries to align with the polarization.

The next parameter of interest is that of particle rotation, Ω , which can be seen in Fig. 5. Looking at the graph of force shows force in the x-direction is maximized when the long axis of the particle is aligned with the fringes, $\Omega = -90^\circ, 90^\circ$, and minimized when the long axis is perpendicular to the fringes. Why this occurs is not fully understood or expected, and further investigation is needed to better understand this situation. The graph of torque however shows a torque which is zero when any of the axes of the particle are aligned with the fringes, which is generally expected. Also the particle experiences maximum torque when the axis are at slightly larger than a 45° angle to the fringes. This is mainly due to the non-uniformity of the field where the particle is located as well as the elongated geometry of the particle itself.

An interesting parameter to examine is that of the grating period, Λ , seen in Fig. 6. In the graph of force, it can be seen that a large force is experienced by the particle when the period is roughly the same order as that of the particle. As the period becomes much larger, the force tends to zero, which is to be expected, as this situation leads to an increasingly reduced gradient of the electric field. The force shown in the region where the period is much smaller than the particle size is not to be trusted as it is most likely the result of numerical error. Further investigation to resolve this size regime would imply calculating the force with a larger number of expansion coefficients. In addition the presence of force in the y-direction could be explained by several factors as discussed previously. The torque is seen to increase in the region where the grating period is the same order of magnitude as the particle size, and plateau as the period gets much larger than the particle size, again approximating constant electric field effects. Also the torque shown for periods much smaller than the particle size is not to be trusted for the same reasons as for the force in this size regime.

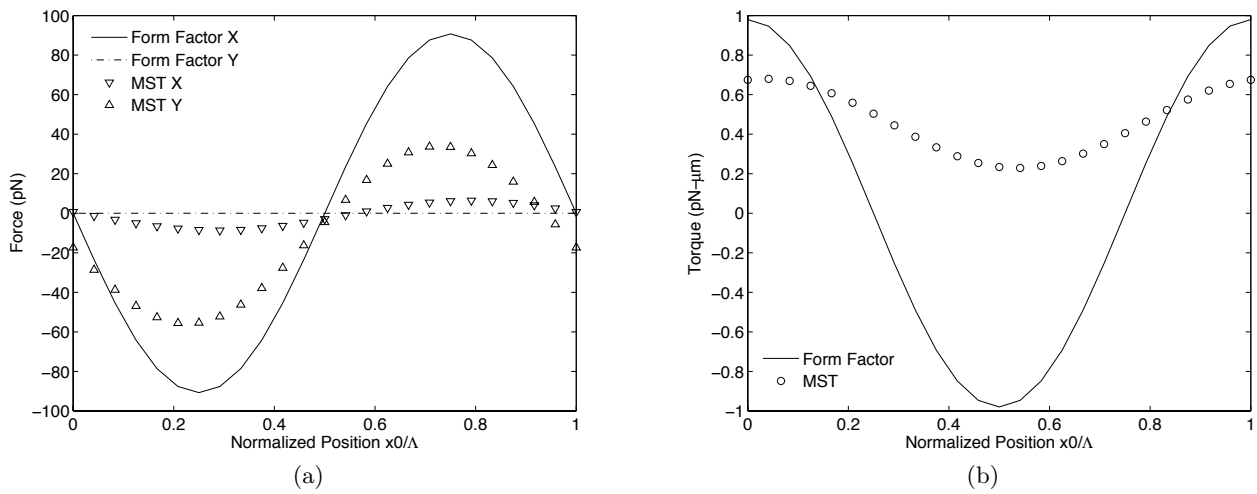


Figure 4. Comparison between form factor and MST force calculations with respect to normalized particle offset in the landscape. $a = 8 \mu\text{m}$, $b = c = 3 \mu\text{m}$, $\epsilon_p = 2.4$, $\epsilon_m = 1.77$, $\Lambda = 16 \mu\text{m}$, $E_0 = 10^6 \frac{\text{V}}{\text{m}}$, and $\Omega = 45^\circ$.

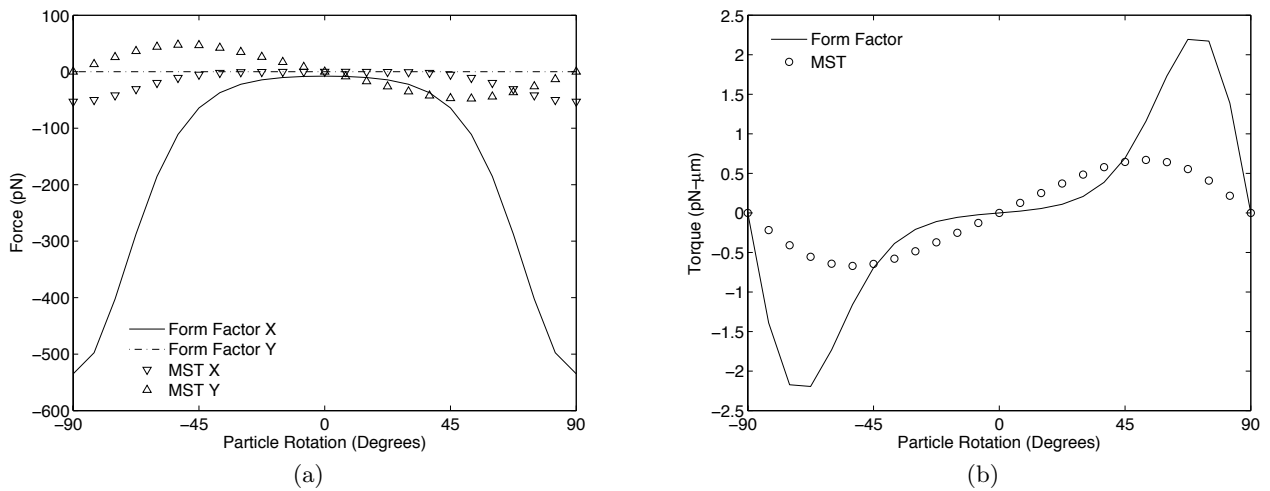


Figure 5. Comparison between form factor and MST force calculations with respect to the particle rotation within the landscape. $a = 8 \mu\text{m}$, $b = c = 3 \mu\text{m}$, $\epsilon_p = 2.4$, $\epsilon_m = 1.77$, $\Lambda = 16 \mu\text{m}$, $E_0 = 10^6 \frac{\text{V}}{\text{m}}$, and $x_0/\Lambda = 1/8$.

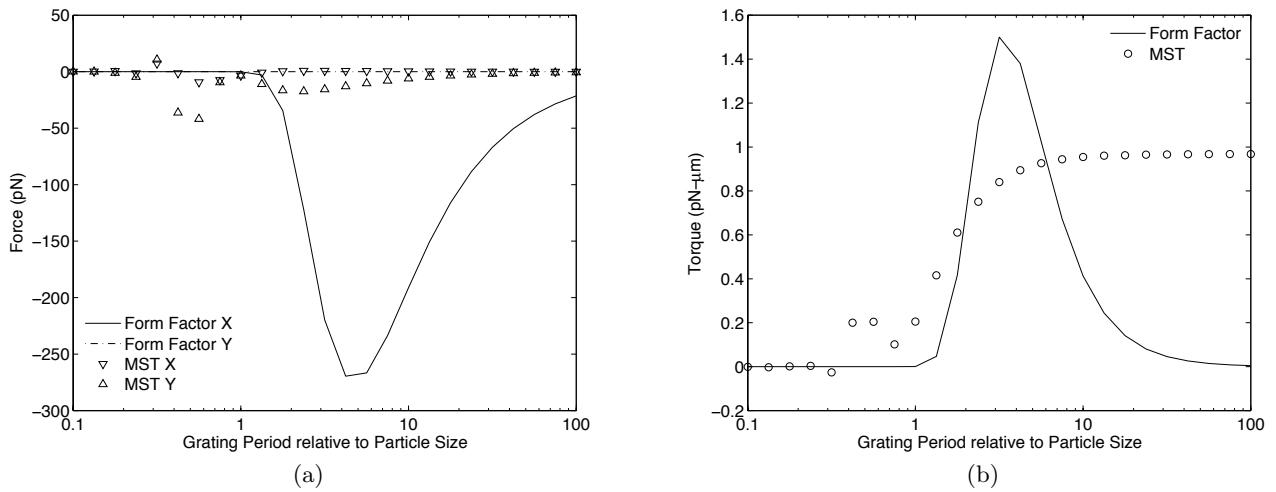


Figure 6. Comparison between form factor and MST force calculations with respect to the relative size of the landscape period. $a = 8 \mu\text{m}$, $b = c = 3 \mu\text{m}$, $\epsilon_p = 2.4$, $\epsilon_m = 1.77$, $E_0 = 10^6 \frac{\text{V}}{\text{m}}$, $\Omega = 45^\circ$, and $x_0/\Lambda = 1/8$.

3.3 Form Factor Comparison

We now examine a comparison between the MST calculation and the form factor method described earlier. In examining the particle position as in Fig. 4, it can be seen that the two methods predict similar values and shape for force. The exception to their similarity would be the y-value of force predicted by the MST, the cause of which is discussed in the previous section. The two differ in their values of torque with respect to particle position, with the form factor method predicting a torque that changes signs depending on position. However the reason for the MST predicted torque being one sign at all positions was discussed in the previous section, and since the form factor method does not account for polarization of the field, some differences in the force and torque should be expected. Examining their predictions for force, as seen in Fig. 5, it can be seen again that their main difference lies in the magnitude predicted by each method, with the MST predicted force being a full order of magnitude smaller than that predicted by the form factor. Although the shapes of the force predicted by the two methods agree, as mentioned in the previous section, further investigation is needed to understand why this shape should occur. The torque predicted by each model matches fairly closely, although the form factor method predicts vastly larger torques when the particle is at an angle of around 45° to 90° . Again it could be that the field polarization has something to do with the difference in shapes of torque predicted by each model. Looking at a change in grating period, Λ , as in Fig. 6, it can be seen that both methods show a peak in both force and torque when the grating period is roughly the same order of magnitude as the size of the particle. The form factor method however shows both force and torque going to 0 as the grating period becomes much larger than the particle size. While for the case of force this is to be expected, torque should generally increase asymptotically as the grating period increases moving towards a constant electric field.

The differences between the form factor method and the MST method in each of the graphs is almost certainly due to the field polarization and the fact that the form factor method does not take into account the field polarization. To this extent, the MST method addresses certain situations of the particle in the optical field that the form factor ignores because of its lack of polarization. Hence the inclusion of polarization into the calculation of force and torque makes a significant contribution to the end result.

4. CONCLUSIONS

Optical trapping is a technology which is receiving a great deal of attention currently, however the theoretical aspects of optical trapping, especially in dealing with ellipsoidal particles has thus far received very little. We developed a calculation of force and torque on spheroidal dielectrics in a general non-uniform optical field using

electrostatic principles and the Maxwell stress tensor. We first solved for the total electric field around the particle using the spheroidal harmonics to aid in solving the boundary conditions. We then used this electric field in the MST to calculate force and torque. Our calculation using the MST gave promising results which generally agreed with previous work for similar situations. The MST calculations also displayed the interesting contributions of the field polarization into the force and torque exhibited on the particle. In comparing these results to those predicted by the form factor method, which does not take into account polarization, there were large similarities, but there were also many areas where the two differed. These differences appear to highlight the significance of including polarization in the calculation of force and torque on the particle.

ACKNOWLEDGMENTS

The authors gratefully acknowledge support from the National Science Foundation REU program (grant ECCS-0733471), and from a U.S. Department of Education GAANN Fellowship.

REFERENCES

- [1] Ashkin, A., Dziedzic, J. M., Bjorkholm, J. E., and Chu, S., "Observation of a single-beam gradient force optical trap for dielectric particles," *11*, 288–290 (1986).
- [2] Grier, D. G., "A revolution in optical manipulation," *Nature* **424**, 810–816 (2003).
- [3] MacDonald, M. P., Spalding, G. C., and Dholakia, K., "Microfluidic sorting in an optical lattice," *Nature* **426**, 421–424 (2003).
- [4] Rogers, J. A., "Organizing nanowires," *Nature Photonics* **2**, 69–70 (2008).
- [5] Lermé, J., Bachelier, G., Billaud, P., Bonnet, C., Broyer, M., Cottancin, E., Marhaba, S., and Pellarin, M., "Optical response of a single spherical particle in a tightly focused light beam: application to the spatial modulation spectroscopy technique," *Journal of the Optical Society of America A* **25**(2), 493–514 (2008).
- [6] Bishop, A. I., Nieminen, T. A., Heckenberg, N. R., and Rubinsztein-Dunlop, H., "Optical application and measurement of torque on microparticles of isotropic nonabsorbing material," *Physical Review A* **68**(033802), 1–8 (2003).
- [7] Grzegorzczuk, T. M. and Kong, K. A., "Analytical expression of the force due to multiple tm plane-wave incidences on an infinite lossless dielectric circular cylinder of arbitrary size," *Journal of the Optical Society of America B* **24**(3), 644–652 (2007).
- [8] Paul, R. and Kaler, K. V. I. S., "Effects of particle shape on electromagnetic torques: A comparison of the effective-dipole-moment method with the maxwell-stress-tensor method," *Physical Review E* **48**(2), 1491–1496 (1993).
- [9] Rockstuhl, C. and Herzig, H. P., "Calculation of the torque on dielectric elliptical cylinders," *Journal of the Optical Society of America A* **22**(1), 109–116 (2005).
- [10] Pelton, M., Ladavac, K., and Grier, D. G., "Transport and fractionation in periodic potential-energy landscapes," *Physical Review E* **70** (2004).
- [11] Conover, B. L. and Escuti, M. J., "The response of particles with anisotropic shape within an optical landscape and laminar flow," *Proceedings of SPIE* **6326**(632614), 1–10 (2006).
- [12] Al-Jarro, A., Paul, J., Thomas, D. W. P., Crowe, J., Sawyer, N., Rose, F. R. A., and Shakesheff, K. M., "Direct calculation of maxwell stress tensor for accurate trajectory prediction during dep for 2d and 3d structures," *Journal of Physics D: Applied Physics* **40**, 71–77 (2007).
- [13] Wang, X., Wang, X.-B., and Gascoyne, P. R. C., "General expressions for dielectrophoretic force and electrorotational torque derived using the maxwell stress tensor method," *Journal of Electrostatics* **39**, 277–295 (1997).
- [14] Barton, J. P., Alexander, D. R., and Schaub, S. A., "Theoretical determination of net radiation force and torque for a spherical particle illuminated by a focused laser beam," *Journal of Applied Physics* **66**(10), 4594–4602 (1989).
- [15] Collett, W. L., Ventrice, C. A., and Mahajan, S. M., "Electromagnetic wave technique to determine radiation torque on micromachines driven by light," *Applied Physics Letters* **82**(16), 2730–2732 (2003).

- [16] Simpson, S. H. and Hanna, S., “Optical trapping of spheroidal particles in gaussian beams,” *Journal of the Optical Society of America A* **24**(2), 430–443 (2007).
- [17] Jackson, J. D., [*Classical electrodynamics*], New York, 3rd ed. (1999).
- [18] Landau, L. D. and Lifshitz, E. M., [*Electrodynamics of continuous media*], Oxford, 2nd ed. (1984).
- [19] Sten, J. C.-E., “Ellipsoidal harmonics and their application in electrostatics,” *Journal of Electrostatics* **64**, 647–654 (2006).
- [20] Moon, P. H., [*Field theory handbook: Including coordinate systems, differential equations, and their solutions*], Springer-Verlag, 2nd ed. (1988).
- [21] Hobson, E. W., [*The theory of spherical and ellipsoidal harmonics*], New York (1965).
- [22] Washizo, M., “Equivalent multipole-moment theory for dielectrophoresis and electrorotation in electromagnetic field,” *Journal of Electrostatics* **62**, 15–33 (2004).